A New MIMO HF Data Link: Designing for High Data Rates and Backwards Compatibility

Robert C. Daniels and Steven W. Peters
{robert.daniels,steven.peters}@kumasignals.com

***Abstract*—High frequency (HF) radios (the 3–30 MHz range) provide tactical communications with the ability to communicate over long distances and around large obstructions without supporting infrastructure (e.g., satellite links). Unfortunately, spectrum is scarce in the low HF operating frequencies. To improve spectral efficiency, commercial UHF/SHF systems have offered multiple antennas with intelligent signal processing (MIMO). MIMO not only amplifies spectral efficiency, but also reduces transmit power, rejects jamming, and increases link reliability. In a companion paper, we demonstrated HF MIMO feasibility with compact cross-polarized arrays through measurements [1]. In this paper, we leverage those measurements to design a new MIMO HF physical layer based on the existing single-antenna MIL-STD-188-110C-Appendix-D wideband HF standard. We include simulation results based on our channel measurements to show that this new standard provides 116% improvement in overall throughput and a 15 dB signal-to-noise ratio (SNR) improvement over the highest-rate single-antenna modes due to greater reliability and reduced sensitivity to amplifier nonlinearities.**

I. Introduction

High frequency (HF) radios are often used in military deployments to provide voice connectivity in remote satellite-denied environments through sky-wave propagation. HF data rates are currently too low to support reliable video or other data-intensive communication because of low bandwidth allocations and challenging propagation conditions. While recent efforts have resulted in new waveforms designed for wider bandwidths and higher data rates, the highest rates are only achievable in the most favorable conditions [2]. These conditions will not be consistently observed due to the variability of the sky-wave channel. Further, extending HF rates through bandwidth expansion is increasingly difficult given the scarcity of acquirable HF spectrum and the challenges of changing international spectrum policy.

One approach to significantly increase data rates without expanding the spectral footprint is to utilize multiple antennas, RF chains, and smart signal processing. This technique, known as multiple-input multiple-output (MIMO), has been successfully deployed in commercial wireless networks to provide multiplicative gains in data rates, robustness to interference, increased link reliability, and reduced transmit power [3].

In a partner paper [1], we validated MIMO in a small-array configuration for challenging near-vertical incidence sky-wave (NVIS) links to resolve feasibility questions that resulted from prior demonstrations of MIMO HF sky-wave communication [4], [5], [6]. Our measurements showed 2.27 times larger data rates, 9 times less transmit power, and >3 times fewer link failures in 2×2 MIMO HF NVIS channels with co-located cross-polarized antennas. This antenna configuration is especially suitable for tactical applications with space constraints. This work also provided critical channel metrics, including spatial correlation matrices, to enable baseband designers to benchmark performance and design MIMO HF protocols.

In this paper, we design a complete physical layer to extend the MIL-STD-188-110C-Appendix-D wideband HF waveform to support 2-antenna MIMO, based on the measurements from [1]. The new waveform doubles the maximum data rate and spectrum efficiency by using spatial multiplexing. Additionally, the reliability of the link is improved using cyclic delay diversity and space-time coding. We provide guidelines for designing a backwards-compatible and practical waveform with all necessary functionality including synchronization, channel estimation, and equalization. Using previously measured channels, simulations of our proposed waveform show that anticipated data rates increase by more than 100%.

II. System Model & Background

This paper uses the discrete-time complex baseband model to complete Monte Carlo simulations for the performance of the proposed MIMO digital HF communications link protocol, as enabled through digital transmit and receive hardware [7]. Let n be the discrete-time index and let $\mathbf{x}[n] \in \mathbb{C}^{2\times 1}$ represent the two complex baseband communication samples transmitted on two transmit antennas, TX 1 and TX 2, respectively. Simultaneously, the receiver captures $\mathbf{y}[n] \in \mathbb{C}^{2\times 1}$ on each of its receive antennas, RX 1 and RX 2, respectively. The receive antennas are assumed to be subject to independent additive complex zero-mean Gaussian random processes with random variable vector $\mathbf{v}[n] \in \mathbb{C}^{2\times 1}$ providing noise samples at time index n such that σ^2 is the noise power on RX 1 and RX 2. The MIMO complex baseband model is completed with

$$\mathbf{y}[n] = \sum_{\ell=0}^{\nu} \mathbf{H}[\ell]\mathbf{x}[n-\ell] + \mathbf{v}[n] \tag{1}$$

where $\mathbf{H}[\ell] \in \mathbb{C}^{2\times 2}$ is the channel matrix with $h_{i,j}[\ell]$ in row i and column j, which represents the impulse response coefficient between TX j and RX i ($i, j \in \{1, 2\}$) at tap delay index $\ell \in \{0, 1, \ldots, \nu\}$. Equation (1) also demonstrates how multiple antenna links exploit MIMO processing through spatial multiplexing and diversity algorithms.

Spatial multiplexing transmission produces independent data streams on TX 1 and TX 2 (e.g., standard spatial multiplexing encodes independent bits into each element of vector $\mathbf{x}[n]$). If the receiver can successfully extract $\{\mathbf{x}[n]\}$ from $\{\mathbf{y}[n]\}$, then two parallel links are observed from a single radio. Spatial multiplexing makes it possible to double the data

Supported in part by Office of Naval Research contract N00014-12-M-0232.
Dr. Daniels and Dr. Peters are with Kuma Signals, LLC, 3520 Executive Center Drive, Suite 120, Austin, TX, 78731-1636.

978-0-7695-5124-1/13 $31.00 © 2013 IEEE
DOI 10.1109/MILCOM.2013.214

rate within a single spectrum allocation. In contrast to spatial multiplexing, diversity algorithms only send a single data stream over both antennas (i.e., sequence $\{\mathbf{x}[n]\}$ is mapped from a scalar sequence). Ideally, with diversity algorithms, the signal from all transmit-receive pairs may be captured, yielding an improved signal-to-noise ratio (SNR), namely the **MIMO SNR** $:= E_s\|\mathbf{H}\|_F^2/(2\sigma_2^2)$ where $\|\cdot\|_F$ is the Frobenius norm and we assume transmit energy is normalized on each transmit antenna. Because channel matrices generally have much more total energy than a single entry, diversity algorithms can substantially boost the SNR, which may be exploited by link adaptation algorithms to increase the data rate [8].[1]

One important feature of MIMO link protocols is the ability to correctly select between diversity and spatial multiplexing modes. Each spatial multiplexing stream, in general, has its own SNR. Stream SNR largely depends on the invertability of channel matrices for the tap indices, ℓ, with most energy. If the channel matrix is poorly scaled with a high condition number, spatial multiplexing will perform poorly since each stream cannot be extracted without severe noise scaling, resulting in poor SNR. Hence, diversity algorithms should be employed in this scenario. Quality of service constraints may also encourage diversity algorithms since the SNR improvement (MIMO SNR) may be leveraged to reduce the transmit power and save energy or reduce radiation footprint during covert operations.

The Monte Carlo simulations that follow in this paper require random generation of MIMO channel matrices, $\mathbf{H}[\ell]$. If a complex Gaussian random variable represents each channel matrix entry, we generally prefer that each matrix entry is statistically independent with unit-variance and zero-mean; this allows for good spatial multiplexing performance. Unfortunately, link geometry often provides substantial statistical correlation between matrix elements, decreasing channel matrix invertability [9]. The correlation between the spatial elements is commonly represented through a covariance matrix

$$\mathbf{Q}[\ell] = \mathbb{E}_{\mathbf{h}}\left[\begin{bmatrix} h_{1,1}[\ell] & h_{2,1}[\ell] & h_{1,2}[\ell] & h_{2,2}[\ell] \end{bmatrix}^T \times \begin{bmatrix} h_{1,1}^*[\ell] & h_{2,1}^*[\ell] & h_{1,2}^*[\ell] & h_{2,2}^*[\ell] \end{bmatrix}\right]. \quad (2)$$

Note that, although each tap delay may exhibit unique spatial correlation values, channel models typically assume the same spatial correlation matrix for each tap, due to array geometry similarities for each multipath response [10]. Until recently, spatial correlation statistics of practical MIMO HF antenna configurations have not been available. In our companion paper, however, channel measurements of cross-polarized horizontal dipole antennas in NVIS channels at 7 MHz have provided narrowband spatial correlation matrices. We use this spatial correlation matrix for simulations in this paper.

III. MIMO Waveform Design

This report will assume MIL-STD-188-110C-Appendix-D as the baseline digital HF waveform [11], summarized in Table I. This baseline digital HF waveform operates on a single carrier with variable constellation configurations (including BPSK, QPSK, 8−PSK, 16−QAM, 32−QAM, 64−QAM, 256−QAM, and a 32-length 8-PSK Walsh sequence). The constellation symbols are transmitted at a variable rate between 2.4 and 19.2 kHz (always an integer multiple of 2.4 kHz) and filtered with a root raised cosine filter with a 35% excess bandwidth factor. This leads to spectrum occupations between 3 and 24 kHz. Forward error correction is accomplished through binary convolutional coding with two generators (with either 7 or 9 constraint lengths) producing a base rate $1/2$ code. Puncturing enables rates of $2/3$, $3/4$, $5/6$, $8/9$, $9/10$, and $9/16$. Cascaded repetition coding enables rates of $1/3$, $1/4$, $1/6$, $1/8$, $1/12$, $1/16$, $2/5$, and $2/7$. The modulation and coding together provides data rates from 75 bps (in 3 kHz spectrum with 32-symbol 8-PSK Walsh sequence) to 120 kbps (in 24 kHz spectrum with 256-QAM and rate $5/6$ coding).

TABLE I. Features of baseline broadband HF waveform (MIL-STD-188-110C-Appx-D) with proposed MIMO extension.

Baseline	**Features**
Modulation	Single carrier: 8−PSK Walsh sequence, PSK, and Shaped QAM for nonlinear power amplifier compatibility
Coding	Punctured binary convolutional (two generators, constraint length 7 or 9) combined with repetition for lower rates
Spectrum Efficiency	$1/32 \rightarrow 20/3$ bits/sec/Hz
Symbol Rate	$2.4 \rightarrow 19.2$ kHz
Spatial Multiplexing	Not available
Data Rate	$0.075 \rightarrow 120$ kbps
Interleaver	Block interleaver over $0.12 \rightarrow 10.24$ seconds
Diversity	Unsupported by waveform, antenna spatial diversity only
Proposed	**Features**
Spatial Multiplexing	**2 data streams** with 1 or 2 code streams
Spectrum Efficiency	$1/32 \rightarrow \mathbf{40/3}$ bits/sec/Hz
Data Rate	$0.075 \rightarrow \mathbf{240}$ kbps
Diversity	**Delay diversity, space-time block coding**

Table I also displays the properties of the proposed MIMO wideband HF waveform, which shows a balance between backwards compatibility with legacy baseline waveform implementations and new features that exploit MIMO to improve performance at all SNR. The most noticeable new feature is the ability to provide spatial multiplexing through the inclusion of two simultaneous data symbol streams. A convention of commercial standards is followed where, when spatial multiplexing is enabled, each stream selects the same constellation and the same coding rate. Results have shown only small gains for allowing greater flexibility [8]. Note that a single code block may operate either over both streams simultaneously or separately. Each scenario is preferable in different operating regimes. For example, a single code stream is desired if each stream exhibits similar SNR values since this allows for larger block lengths. Two code streams are desired if SNR varies between the two streams to increase the probability that at least one stream is decoded correctly.

The proposed waveform also supports diversity mode transmission. Diversity mode will be available through delay diversity mode and space-time block coding (format similar to Alamouti). Delay diversity delays the output of the second transmit antenna by a fixed duration. At the receiver this essentially looks like multipath, converting spatial channel paths into temporal channel paths, which can already be captured in legacy systems [12]. For non-legacy operation, space-time block coding is preferred. Space time block coding intelligently adds redundancy across transmit antennas in a way such that the receiver can capture full channel diversity without knowledge of the channel at the transmitter [3]. Digital beamforming and closed-loop precoding diversity

[1] Here, we do not discuss the difference between diversity gain and array gain. Diversity algorithms with multiple antennas capture *both* array gain and diversity gain when compared to single antenna communication.

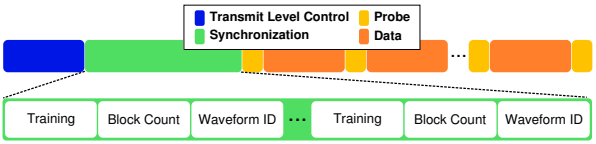

Fig. 1. Frame format of baseline (legacy) MIL-STD-188-110C-Appendix-D wideband HF packets with synchronization field detail.

algorithms have been avoided since the variability of the HF NVIS channel suggests that current network functionality operates on too large of a time scale to make precoding (beamforming) reliable [13]. This may be revisited with justification of channel stability [14].

A. Frame Format

Support of the new features in Table I requires consideration of the frame format for transmitted packets. The baseline format is shown in Figure 1. Each packet begins with transmit level control (TLC) data to allow automatic gain control (AGC) in the receiver and, ultimately, accurate analog-to-digital conversion (ADC). After the TLC sequence, the synchronization field is transmitted. The synchronization field holds three sub-fields, beginning with a fixed training field, which serves two purposes: 1) to allow the receiver to detect the presence of an incoming packet 2) to perform initial time and frequency synchronization. Block Count data is encapsulated into eight bit Walsh sequences in the next field, which can be detected under phase ambiguity (channel estimation unnecessary) through correlative peak detection. Block Count data informs the receiver of how many repetitions of the sub-fields remain. The last sub-field indicates the Waveform ID through ten bits encapsulated into a Walsh sequence (similar to Block Count). The Waveform ID tells the receiver what modulation, coding, and interleaving configuration is required to successfully decode the data fields that follow. Before the data fields, however, a Probe field is transmitted. The Probe field contains fixed training data to allow the receiver to estimate the channel impulse response throughout the packet.

The baseline frame format is only designed for single antenna transmission and cannot be trivially repeated on both transmit antennas. The new (proposed) waveform provides two new frame formats, both inspired by past translations of commercial MIMO standards (IEEE 802.11n and 3GPP-LTE) [12], [15]. In the first (legacy-compatible) MIMO frame format, illustrated in Figure 2 (*top*), the first transmit antenna sends the baseline TLC and Synchronization fields. The second transmit antenna delays sending an exact copy of the TLC and Synchronization by a fixed time period. At the receiver, this appears as multipath. The legacy receiver will synchronize with the strongest multipath component (selected over both transmit antennas). Hence, this mode provides a second set of multipath components for the receiver to synchronize to, increasing the chance of a strong path for successful communication. Due to the geometric similarity of the channel for both transmitters, simultaneous arrival of signals is likely without the included delay. This can have catastrophic consequences, for example, if the phase shift between each transmit antenna path is π radians. To ensure diversity gains in the two transmit antenna

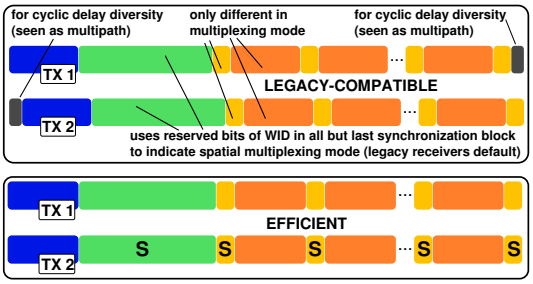

Fig. 2. New (proposed) frame formats for MIMO operation offer backwards compatibility with existing receivers (*top*) and efficient operation (*bottom*). 'S' indicates that shift operations are used as demonstrated in Figure 3.

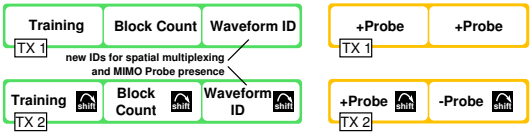

Fig. 3. Synchronization field (*left*) and Probe field (*right*) with efficient frame format in Figure 2 (*bottom*).

scenario, transmission delay on the second antenna is required.

The second (efficient) MIMO frame format is shown in Figure 2 (*bottom*). The drawback of adding a delay to the second transmit antenna in the legacy-compatible frame format is that it reduces the ability to tolerate multipath delay spread. The new frame format eliminates this delay by using different TLC data and cyclically shifting the Synchronization field elements, as demonstrated in Figure 3 (*left*). Note that the receiver must be aware of these cyclic shifts to harness diversity during synchronization, rendering this new frame format incompatible with legacy receiver operation.

The Waveform ID sub-field must be modified to allow for spatial multiplexing modes in both of the new frame formats. In the legacy-compatible format, this implies usage of the reserved bits. The reserved bits will be used in all but the last synchronization block count, causing legacy receivers to determine incorrect decoding of the Waveform ID (which is the desired scenario). Updated (MIMO aware) receivers will know that this indicates spatial multiplexing mode. The last block count will provide the correct modulation and coding scheme. Hence, legacy-compatibility compromises the reliability of synchronization in spatial multiplexing mode. In contrast, modification of the efficient frame format is achieved by adding extra bits to the Waveform ID field.

The remaining characteristics of the proposed frame formats depend on whether spatial multiplexing mode is used during transmission. In diversity-only mode, the legacy-compatible frame format is exactly the same as the baseline system (there are no changes in the probe or data format). The efficient frame format, however, adds a cyclic shift to each probe and each data block. In spatial multiplexing mode, both of the new frame formats use the same probe and data fields. The probe field is highlighted in Figure 3 (*right*). The probe field must allow for estimation of channel impulse responses between a receive antenna and both transmit antennas. This is achieved by repeating the probe field. A sign change is also added to the second transmit antenna. This sign change

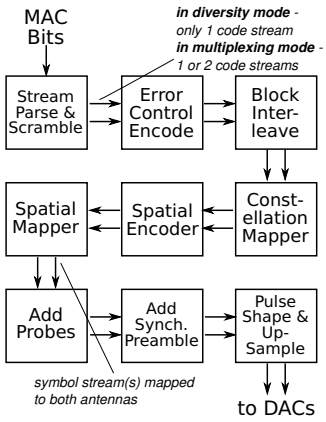

Fig. 4. Process to create samples in the new frame formats of Figure 2.

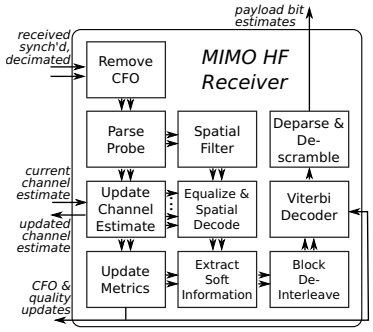

Fig. 5. Block diagram of the data decoding loop of the receiver. This decoding loop occurs for each probe and data symbol.

allows the receiver to combine the blocks (through addition or subtraction) and cancel each of the transmit antennas successively. Note that the data fields do not need to be cyclically shifted since the data and symbols are independent between transmit antennas in spatial multiplexing mode.

B. Transceiver Digital Processing

The digital samples in the new frame formats are created according to the block diagram of Figure 4. Note that the spatial mapper process will likely select an identity matrix transformation. During the transmission process, probe fields are inserted and the synchronization preamble is prepended before pulse shaping and upsampling commence. The last step before RF up-conversion is digital-to-analog baseband conversion on each transmit antenna path.

The first operation of the receiver is to detect the presence of a packet. Several architectures for detection are possible including self-reference correlation (since the TLC sequence is the conjugate of the fixed training field of synchronization) or FFT-based peak detectors of cross-correlated data [16]. FFT-based peak detectors are commonly found in HF digital receivers [17]. The cyclic shifts allow for all transmit-receive paths to be used for detection, although it requires two separate correlation metrics in FFT-based peak detectors. The detection metric for both architectures also provides a coarse estimate of the channel frequency offset (CFO) due to mismatches between the frequency references at the transmitter and receiver.

The samples given to the detection algorithm are assumed to be taken at a rate that is an integer multiple of the symbol rate (i.e., oversampled by an integer factor). A bank of decimated processes are run in parallel to find the sample instance which maximizes the detection peak. This information is given to the remaining blocks in the receiver such that decimation and matched filtering is optimized. Note also that, if the signal quality is high, the peak detection metrics may be used to make subsample adjustments in the ADC. Once a peak is discovered, the rate at which the receiver adjusts its gain slows since fast gain transitions will reduce the quality of channel estimation and equalization algorithms in the receiver.

The data decoding portion of receiver is shown in more detail through Figure 5. Before data can be decoded, the CFO effects are removed. In parallel to any spatial filtering that may be required on each of the data streams, the probe field is analyzed to find channel impulse response information. In HF systems, the impulse response is estimated periodically throughout the data decoding process since the channel evolves throughout a single packet [18]. The uniquely designed channel probes in Figure 3 allow the receiver to add or subtract successive fields in such a way that each transmit-receive path can be evaluated independently. Hence, baseline channel estimation algorithms can be applied for each transmit-receive path. Channel estimation is an ongoing process that is typically accomplished through adaptive filters, such as the popular least means squares (LMS) and Kalman filter algorithms [19].

Data decoding proceeds by using the updated channel estimate. In diversity-only mode the intersymbol interference, caused by excess delay multipath, must be mitigated through equalization. In spatial multiplexing mode the inter-stream interference, caused by the mixing of transmit paths at a single receive antenna, must also be mitigated. There are many different available equalization algorithms for both of these purposes. In the simulations that follow next, frequency domain equalization (FDE) was used in the same form as [20], where FFT operations reduce the complexity of equalizer architectures that satisfy minimum mean square error (MMSE) statistical constraints.[2] Several other options, however, are available, including full maximum likelihood (ML), MIMO decision feedback equalization (MIMO DFE), and MIMO turbo equalization. After equalization the diversity provided by spatial coding is captured through linear transformations.

IV. Simulation Results

Our simulations demonstrate performance gains for the proposed MIMO HF waveform over the baseline. Synchronization and channel estimation are assumed perfect, removing any performance consequences for the frame formats in Figure 2. As discussed in Section II, simulations will use the 58 MIMO NVIS channel measurements captured at 7 MHz and the associated statistical model with spatial correlation from [1]. For ease of interpretation, we include a reduced set

[2]The FFT block includes the data block and the probe that follows each data block. By including the probe in the FFT block, we enable cyclic convolution without a cyclic prefix. The FFT block size depends on the Waveform ID and the bandwidth in the standard. In MIL-STD-188-C-Appx-D the last probe is cyclically shifted causing cyclic convolution violation and FDE degradation. We have not included this cyclic shift in our simulations for simplicity.

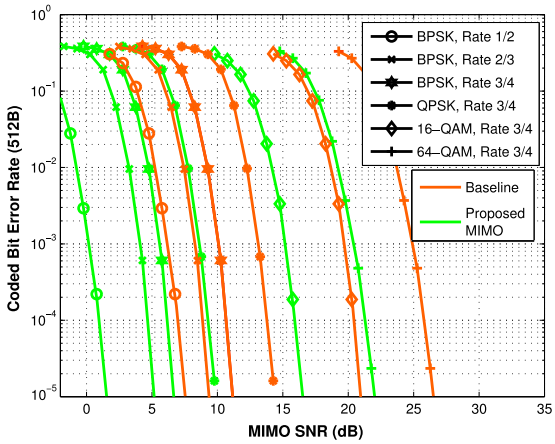

Fig. 6. BER versus MIMO SNR for baseline and proposed HF protocol with space-time block coding diversity and the measurements from [1].

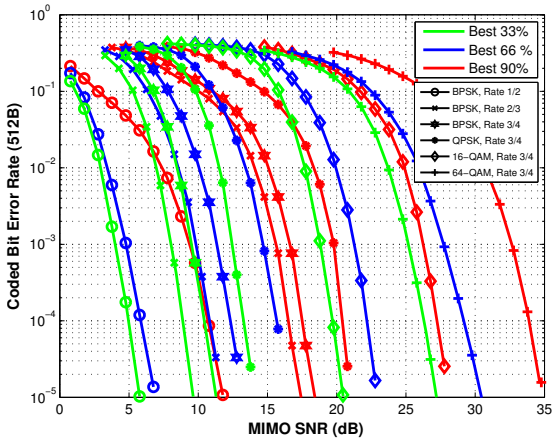

Fig. 7. BER versus MIMO SNR for spatial multiplexing in the proposed HF protocol using the 58 channel measurements from [1].

of modulation and coding schemes. We do not use shaped constellations (PAPR-reduced) in an attempt to reduce computational burden. Figures 6, 7, 8, 10 represent simulations with narrowband (single tap) channels and Figure 9 represents frequency-selective (multiple tap) channel simulations.

First, consider the coded (block size is 512 bytes) bit error rate (BER) performance of baseline HF communication in comparison to the proposed HF MIMO protocol in diversity mode, averaged over all 58 measured channels, in Figure 6. All SNRs are simulated by adjusting the noise variance at the receiver. Note that when MIMO is exploited, 6 **dB in SNR gain results**. For example, from the graph we can see that BPSK with rate 1/2 coding achieves 10^{-5} BER at about 7.5 dB when using a single antenna. When using two antennas at transmitter and receiver, however, the same configuration can achieve the target BER at about 1.5 dB, resulting in 6 dB gain.

Figure 7 shows the BER when spatial multiplexing is implemented in the proposed protocol. Note that if BER was averaged over all 58 channels, the BER would reflect the worst channels due to the high BER that characterizes channels

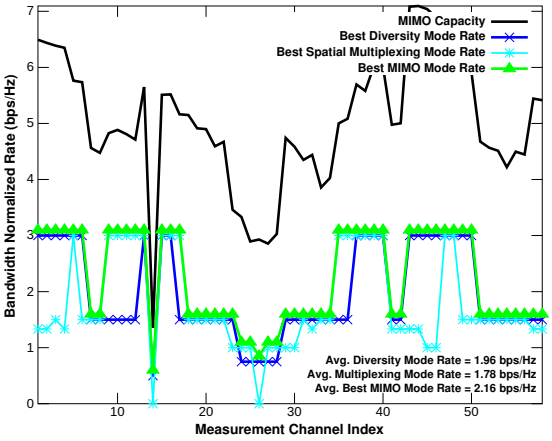

Fig. 8. Spectral efficiency of the measured MIMO channels from [1] (captured over 24 minute period) in proposed HF protocol. Link adaptation toggles between diversity and spatial multiplexing modes for maximal performance.

with poor MIMO matrix invertability. Hence, we separate the BER performance for the best 33%, 66%, and 90% of the MIMO channels. We want to emphasize that these are based on channel measurements, and thus the conditions in which spatial multiplexing is favored over diversity modes will vary. Not all HF channels are suitable for spatial multiplexing. Transmit mode adaptation (link adaptation) is required to switch between diversity mode operation and spatial multiplexing.

Figure 8 plots the adapted rate of the proposed procotol (BER $= 10^{-5}$ required) over time along with diversity mode rate, spatial multiplexing rate, and MIMO channel capacity in the 58 measured channels. The achievable rates are below capacity because of finite constellations, non-Gaussian signaling, and finite block lengths. A key takeaway is that a MIMO system must intelligently adapt between modes to maximize reliability and data rate. If only diversity mode is used, the average spectral efficiency is 1.96 bps/Hz. If only spatial multiplexing mode is used, it is 1.78 bps/Hz. With optimal adaptation between both modes, the average spectral efficiency is 2.16 bps/Hz, a $10-21\%$ increase. For comparison, optimal adaptation in the baseline yielded a spectral efficiency of 1.00 bps/Hz. Hence, the proposed MIMO HF protocol provides an average **116% rate gain** *in measured channels*. This is not surprising, as this is predicted by capacity [1].

Each of the simulations presented thus far have been based on measured channels using a single tap since the measurements were narrowband. The general conclusions drawn from these plots are applicable to multipath channels with excess delay spread (wideband), but the actual performance numbers will be different. To demonstrate the differences, we have considered a 2-tap channel with delay spread of 2 ms and equal average energy on each tap (the Waterson model). This is a challenging channel and falls under the umbrella of ITU-R Poor channels. To extend the measurements to multiple taps, we utilize a statistical channel model that exploits the correlation matrix in [1] derived from the measurements. This models incorporates all potential channel conditions, including some channels that have a very unfavorable condition number. Figure 9 shows performance of spatial multiplexing in 48 kHz channels. 48 kHz was chosen since it represents proposed

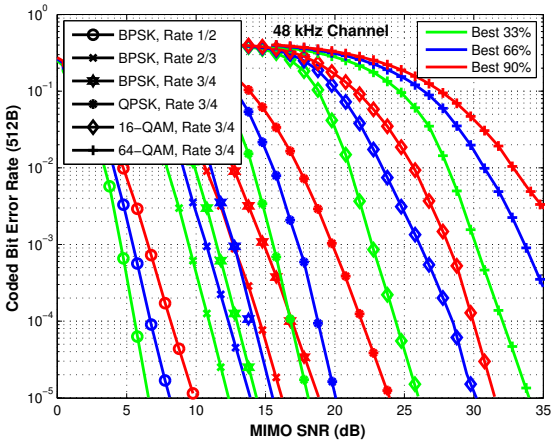

Fig. 9. MIMO 48 kHz Performance with spatial multiplexing.

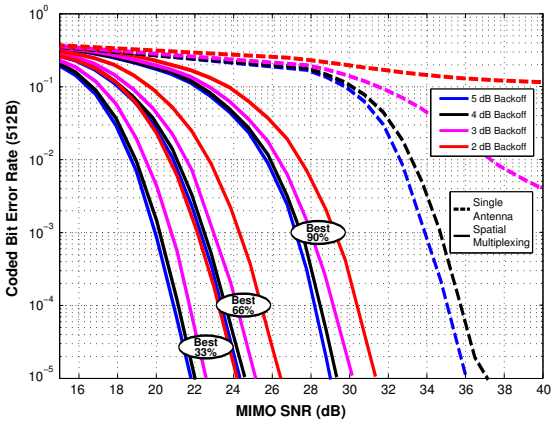

Fig. 10. BER of 2-stream 16-QAM (spatial multiplexing) and single-antenna 256-QAM (baseline) in the face of amplifier nonlinearities.

spectrum allocation in future wideband HF standardization.

One benefit of spatial multiplexing that is often overlooked is its performance advantage under power amplifier nonlinearities. For example, to achieve 6 bps/Hz, the baseline single-antenna system uses 256-QAM with rate $3/4$ coding. This not only requires a very high SNR for error-free transmission, but also has an excessively high peak-to-average power ratio (PAPR). A high PAPR means the transmitter must reduce its average transmit power to ensure that the waveform will be minimally distorted during waveform peaks. Figure 10 shows the BER for 6 bps/Hz communication under various backoff levels in the presence of PA nonlinearities (standard Rapp amplifier model with parameter value $p = 2$ to accurately model typical HF amplifiers). For the single-antenna case 36 dB SNR is needed with 5 dB PA backoff.[3] Figure 10 demonstrates that with MIMO, however, we can transmit the exact same data rate at 13 **dB lower SNR and** 2 **dB less backoff**, an effective gain of 15 dB. Hence, the baseline protocol requires a 100 W power amplifier for communication at 6 bps/Hz, our MIMO protocol will only require two ≈ 3 W power amplifiers (in good channels). In poorly-conditioned channels we still observe an 8 dB gain.

[3]Constellation shaping can reduce PAPR at the cost of increased BER.

V. Conclusion

MIMO offers HF links increased spectral efficiency, reduced transmit power, interference/jamming robustness, and extended reliability. In this paper, we design a new HF physical layer protocol to provide the full capabilities of 2-antenna MIMO and backwards compatibility with MIL-STD-188-110C-Appendix-D. Link simulations that use channel measurements in challenging NVIS conditions show staggering performance. The new protocol increases achievable data rate by $> 100\%$ and improves BER performance by up to 15 dB SNR over equivalent single-antenna communication due to greater reliability and reduced amplifier sensitivity.

References

[1] R. C. Daniels, S. W. Peters, and R. W. Heath, Jr., "HF MIMO NVIS measurements with colocated dipoles for future tactical communications," in *IEEE MILCOM*, 2013.

[2] M. B. Jorgenson *et al.*, "Implementation and on-air testing of a 64 kbps wideband HF data waveform," in *IEEE MILCOM*, 2010.

[3] D. Gesbert and J. Akhtar, "Breaking the barriers of Shannon's capacity: An overview of MIMO wireless systems," *Signal Processing*, 2002.

[4] S. Gunashekar *et al.*, "Investigations into the feasibility of MIMO techniques within the HF band: Preliminary results," *Radio Science*, vol. 44, no. 1, 2009.

[5] P. M. Ndao *et al.*, "Capacity estimation of MIMO ionospheric channels," in *Ionospheric Radio Systems and Techniques*, 2009.

[6] A. Forenza, R. W. Heath, Jr., S. G. Perlman, R. Van Der Laan, and J. Speck, "System and method for distributed input distributed output wireless communications," *US Patent Application 20080080631*, 2008.

[7] W. Tranter *et al.*, *Principles of communication systems simulation with wireless applications*. Prentice Hall Press, 2003.

[8] R. C. Daniels, "Machine learning for link adaptation in wireless networks," Ph.D. dissertation, The University of Texas at Austin, 2011.

[9] A. Van Zelst and J. S. Hammerschmidt, "A single coefficient spatial correlation model for MIMO radio channels," in *URSI General Assembly*, 2002, pp. 17–24.

[10] J. Kermoal *et al.*, "A stochastic MIMO radio channel model with experimental validation," *IEEE Journal on Selected Areas in Communications*, vol. 20, no. 6, pp. 1211–1226, 2002.

[11] W. N. Furman and J. W. Nieto, "Latest on-air testing of US MIL-STD-188-110C appendix D wideband HF data waveforms," in *International Conference on Ionospheric Radio Systems and Techniques*, 2012.

[12] X. Yang, "IEEE 802.11n: enhancements for higher throughput in wireless LANs," *IEEE Wireless Communications*, vol. 12, no. 6, pp. 82–91, 2005.

[13] L. Wagner and J. Goldstein, "Channel spread parameters for the high-latitude, near-vertical-incidence-skywave HF channel: Correlation with geomagnetic activity." DTIC Document, Tech. Rep., 1995.

[14] R. C. Daniels *et al.*, "Throughput/delay of limited feedback beamforming in indoor wireless networks," in *IEEE GLOBECOM*, 2008.

[15] D. Astély *et al.*, "LTE: the evolution of mobile broadband," *IEEE Communications Magazine*, vol. 47, no. 4, pp. 44–51, 2009.

[16] J. Heiskala and J. Terry, *OFDM wireless LANs: a theoretical and practical guide*. SAMS publishing, 2002.

[17] J. Provolt, "Architecture and debugging of digital signal processing software in a high frequency MIL-STD-188-110A single tone receiver," Master's thesis, Iowa State University, 2008.

[18] L. Lindbom, "Simplified Kalman estimation of fading mobile radio channels: High performance at LMS computational load," in *IEEE ICASSP*, vol. 3, 1993, pp. 352–355.

[19] A. Sayed, *Fundamentals of adaptive filtering*. Wiley-IEEE Press, 2003.

[20] J. P. Coon and M. A. Beach, "An investigation of MIMO single-carrier frequency-domain MMSE equalization," in *London Communications Symposium*, 2002, pp. 237–240.